EARTH SURFACE PROCESSES AND LANDFORMS
Earth Surf. Process. Landforms **41**, 1199–1210 (2016)

Published online 11 February 2016 in Wiley Online Library
(wileyonlinelibrary.com) DOI: 10.1002/esp.3894

Pressure and shear stress caused by raindrop impact at the soil surface: Scaling laws depending on the water depth

Amina Nouhou Bako,[1,2]* Frédéric Darboux[1†], François James,[2] Christophe Josserand[3] and Carine Lucas[2]
[1] INRA, UR0272, UR Science du sol, Centre de recherche Val de Loire, F-45075 Orléans, France
[2] MAPMO, UMR CNRS 7349, Fédération Denis Poisson, FR CNRS 2964, Université d'Orléans, F-45067 Orléans, France
[3] Sorbonne Universités, CNRS & UPMC Université Paris 06, UMR 7190, Institut Jean Le Rond d'Alembert, F-75005 Paris, France

Received 21 May 2015; Revised 23 November 2015; Accepted 14 December 2015

*Correspondence to: Amina Nouhou Bako, INRA, UR0272, UR Science du sol, Centre de recherche Val de Loire, F-45075 Orléans, France. E-mail: amina.nouhou-bako@orleans.inra.fr
[†]Current address: INRA, Laboratoire Sols et Environnement, UMR 1120, Vandoeuvre-lès-Nancy, F-54518, France

ESPL
Earth Surface Processes and Landforms

ABSTRACT: Raindrop impact is an important process in soil erosion. Through its pressure and shear stress, raindrop impact causes a significant detachment of the soil material, making this material available for transport by sheet flow. Thanks to the accurate Navier–Stokes equations solver Gerris, we simulate the impact of a single raindrop of diameter D, at terminal velocity, on water layers of different thickness h: $\frac{D}{10}$, $\frac{D}{5}$, $\frac{D}{3}$, $\frac{D}{2}$, D, $2D$, in order to study pressures and shear stresses involved in raindrop erosion. These complex numerical simulations help in understanding precisely the dynamics of the raindrop impact, quantifying in particular the pressure and the shear stress fields. A detailed analysis of these fields is performed and self-similar structures are identified for the pressure and the shear stress on the soil surface. The evolution of these self-similar structures are investigated as the aspect ratio h/D varies. We find that the pressure and the shear stress have a specific dependence on the ratio between the drop diameter and the water layer thickness, and that the scaling laws recently proposed in fluid mechanics are also applicable to raindrops, paving the road to obtain effective models of soil erosion by raindrops. In particular, we obtain a scaling law formula for the dependence of the maximum shear stress on the soil on the water depth, a quantity that is crucial for quantifying erosion materials. Copyright © 2016 John Wiley & Sons, Ltd.

KEYWORDS: raindrop; Navier–Stokes equations; pressure; shear stress

Introduction

Raindrop impact is a major driver of soil erosion and acts through a wide range of processes (Terry, 1998; Planchon and Mouche, 2010): the raindrop impacts break down aggregates, leading to soil detachment and crust formation (Bresson and Moran, 2003). They also cause splashes, i.e. the transport of soil material in the air over distances of a few decimeters (Leguédois *et al.*, 2005). Also, raindrop impacts are essential in shallow overland flow (i.e. sheet flow) for the detachment of particles. Indeed, sheet flow by itself does not have the ability to detach particles because of its limited velocity and thus weak shear stress (Kinnell, 1991). The impacts of the raindrops can detach material, which is then transported by the sheet flow.

Drop impact effects can differ strongly depending on whether the soil is dry or wet, because both the shear strength of the soil and the shear stress caused by the drops depend on the soil humidity. For raindrops, the soil can be considered to be wetted rapidly, so we will focus here on the impact on a thin liquid film. The presence of a thin water layer at the soil surface modifies the effect of raindrop impacts (Kinnell, 1991). The consequences of drop impacts depend primarily on drop properties. However, the drops of concern for soil erosion have a narrow range of features: raindrops are consided at terminal velocity, leading to a clear relationship between diameter and velocity (Atlas *et al.*, 1973). This contrasts with other usual applications in fluid mechanics (e.g. ink-jet printing, where the ink drop impacts the paper or the coating of a surface by multiple drop impacts) where drops vary in viscosity, density, surface tension, velocity and diameter (Marengo *et al.*, 2011).

Raindrop-driven erosion depends also on soil properties such as soil resistance to shear stress (Sharma *et al.*, 1991; Mouzai and Bouhadef, 2011), hydrophobicity (Ahn *et al.*, 2013) and roughness (Erpul *et al.*, 2004). While raindrop impacts cause splashes, the quantity of eroded material is controlled mostly by the shear created by the impact, which is not strongly affected by the splash itself (Josserand and Zaleski, 2003). Indeed, it has been argued that the erosion, in terms of bedload transport rate, is controlled by the shear stress affected at the soil boundary, usually measured through the dimensionless Shields number (Parker, 1990; Charru *et al.*, 2004; Houssais and Lajeunesse, 2012). Although these results have been deduced precisely for gravel river beds made of non-cohesive granular materials with a narrow granulometric distribution, it is believed that this bed shear stress, and to a

smaller extent the bed pressure, are the main ingredients of most erosion processes. Therefore, if the transport of eroded materials can be influenced by the splashing itself, which is always present for raindrop impact, the bedload transport rate is primarily due to the shear stress created by the impact.

The influence of the water layer on the erosion process has also drawn attention: first, one could argue that the erosion is limited by the shielding of the soil surface by the water layer. Raindrop energy is absorbed by the water layer, which lowers the pressure and shear stress exerted on the soil. It has been documented, in fact, that a water layer can maximize sheetflow erosion rate in comparison to a drained surface and that such erosion depends mostly on the ratio between the water depth and the raindrop diameter (Singer *et al.*, 1981). In fact, there is a critical depth h_c at which the splash transport rate is maximal: beyond h_c the transport rate decreases strongly. However, different values for h_c have been proposed in the literature, as shown in (Dunne *et al.*, 2010): for instance, it can vary from $h_c = D$ (Palmer, 1963, 1965) to $h_c = 0.2D$ in Torri and Sfalanga (1986), and even by $0.14D \leq h_c \leq 0.2D$ according to Mutchler and Young (1975). Finally, Ghadiri and Payne (1986) showed a reduction of soil splash once a water layer covered the soil surface, while Moss and Green (1983) and Kinnell (1991) found that the outflow rate of raindrop-induced flow transport reached its maximum value when the flow depth equaled two to three drop diameters. For three drop diameters (and above), detachment by raindrops becomes quite limited but drop energy still allows for particle suspension, leading to a significant transportation rate (Ferreira and Singer, 1985).

Raindrop interaction with the soil surface has been investigated using numerical simulations (Wang and Wenzel, 1970). They allow for the computation of pressure and shear stress fields at the soil surface (Huang *et al.*, 1982; Ferreira *et al.*, 1985; Hartley and Alonso, 1991; Hartley and Julien, 1992). All these simulations considered a rigid soil surface, hence not accounting for the elasticity of the soil or its granular nature. According to Ghadiri and Payne (1986), the soil behaves like a solid during the short time of the impact, justifying the simplification. These simulations have enabled the determination of critical variables. For example, maximum shear stress was found to depend mostly on the Reynolds number and the water layer thickness-drop diameter ratio (Hartley and Alonso, 1991; Hartley and Julien, 1992). However, owing to limitations in computer and algorithm performance, simulations were carried out with critical parameters (such as the Reynolds number) well outside the natural range, moderating confidence in the results.

The present paper takes advantage of the recent developments of detailed and direct simulations in fluid mechanics to study the impact of single raindrops on a soil surface with a water layer (see reviews on drop impacts in the fluid mechanics literature: Rein, 1993; Yarin, 2006; Marengo *et al.*, 2011; Josserand and Thoroddsen, 2016). The pressure field inside the water layer, the pressure field at the soil surface and the shear stress at the soil surface are analyzed for raindrops of diameter 2 mm and terminal velocity 6.5 m s^{-1}, varying the thickness of the water layer. Short timescales are considered, i.e. development of stresses before particle splash initiation. A self-similar approach valid for a thin liquid layer is used to analyze the results, showing that scaling laws recently proposed in fluid mechanics apply to natural raindrops too. It confirms that the ratio between water depth and raindrop diameter is critical in order to understand the effect of raindrop impact.

Materials and Methods

Problem configuration

We consider the normal impact of a liquid drop of diameter D on a thin liquid film of thickness h in the paradigm of rainfall (Figure 1). The liquid has a density and dynamic viscosity denoted by ρ_l and μ_l respectively. The density and viscosity of the surrounding gas are denoted by ρ_g and μ_g. The drop impacts on the ground at velocity $\mathbf{U} = -U_0\mathbf{e}_z$, which corresponds to the terminal velocity for a raindrop. We will assume here for the sake of simplicity that the raindrop has a spherical shape, even though it is known that raindrops can have a deformed shape, particularly for large diameters (Villermaux and Bossa, 2009). However, it is not expected to impact the dynamics significantly, and the effect of the specific shape of the impacting drop is postponed to future work. The gravity is denoted by $\mathbf{g} = -g\mathbf{e}_z$, and the liquid–gas surface tension by γ.

Different dimensionless parameters can be constructed in this configuration. Two of them are commonly used in drop impact problems, since they characterize the balance between the inertia of the drop with the viscous and capillary forces respectively: firstly, the Reynolds number (Re) is the ratio between inertia and viscous forces:

$$\mathrm{Re} = \frac{\rho_l U_0 R}{\mu_l}$$

For raindrops, Re ranges from 6500 to 23 000 (Hartley and Julien, 1992). Secondly, the Weber number (We) is defined as the ratio between inertia and capillary forces:

$$\mathrm{We} = \frac{\rho_l U_0^2 R}{\gamma}$$

The Weber number ranges from 50 (for a raindrop diameter of 0.5 mm and a velocity of 2 m/s) to 12 000 (for a raindrop diameter of 6 mm and a velocity of 9 m/s) for natural rainfall. The problem depends also on the aspect ratio of the problem geometry, i.e. the ratio between the drop diameter and the thickness of the liquid film:

$$\frac{h}{D}$$

Additional dimensionless numbers are present in this problem, but are of limited interest, either because they do not depend on the raindrop impact configuration, or because they characterize a physical mechanism that can be neglected here. This is the case with the Froude number:

$$\mathrm{Fr} = \frac{U_0^2}{gD}$$

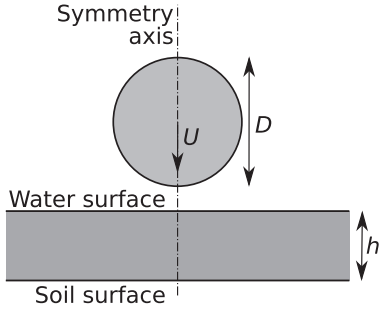

Figure 1. Schematic configuration of a raindrop (diameter D and terminal velocity U) impacting a water layer of depth h.

which quantifies the ratio between inertia and gravity forces; it can take values between 800 and 1400 for natural rainfall. Indeed, although gravity is crucial to accelerate the raindrop to its terminal velocity, gravity itself plays quite a limited role in the impact dynamics and hence is usually not accounted for in the modeling and numerical simulation of drop impacts (Josserand and Zaleski, 2003). For instance, for a drop falling from a height H, the free-fall velocity gives $U_0^2 \sim 2gH$, so that the Froude number is simply the ratio $2H/D$. Since the terminal velocity of a raindrop is equivalent to a free-fall height H of several meters, the Froude number will always be very high in the present problem. Note, finally, that while the Reynolds and Weber numbers are also high in the present problem, this does not mean that viscous and capillary effects can be neglected: the formation of a thin liquid layer means that viscous and capillary effects will be important in some region of the flows – something that is not valid for gravity, which can thus be safely neglected.

The two dimensionless numbers related to the liquid/gas properties, namely the density ratio ρ_g/ρ_l and the viscosity ratio μ_g/μ_l, present a limited interest too: while the surrounding gas can sometimes influence the splashing properties (Xu *et al.*, 2005), in particular through the entrapment of an air bubble beneath the drop on impact (Thoroddsen *et al.*, 2003, 2005), this effect is negligible for the impact of a raindrop (Hartley and Alonso, 1991). Moreover, these two dimensionless numbers are only related to the gas and liquid characteristics and not to the impact conditions. Therefore they do not vary significantly with the raindrop radius and velocity.

Based on the water hammer pressure, i.e. the pressure created by the inertia of the drop hitting a solid surface, it was first suggested in the soil erosion literature that the amplitude of the stress on the soil surface can be quite large (2–6 MPa), with a limited duration of about 50 μs (Ghadiri and Payne, 1980), this duration increasing with the depth of the water layer (Ghadiri and Payne, 1986). However, such high water hammer pressures have not been observed experimentally (Ghadiri and Payne, 1986; Hartley and Julien, 1992; Josserand and Zaleski, 2003) and, following the argument of Ghadiri and Payne (1980), it can be shown that this pressure should arise only during a very short time of the order of D/c (where D is the drop diameter and c is the sound speed), leading to a typical timescale of the order of 1 μs as found by Ghadiri and Payne (1986). Then, the pressure decreases rapidly with time as shown in numerical simulations (Josserand and Zaleski, 2003). Moreover, as discussed by Nearing *et al.* (1986, 1987), compressible effects can be neglected since they will only influence the very early time of contact and a very small region of the impacted zone. This is in agreement with former theoretical and experimental studies on drop impacts where compressible effects were shown to appear only at much higher drop velocities, typically of the order of a fraction of the sound velocity in water (Lesser and Field, 1983). Therefore, as shown and as used in recent studies, the liquid can be assumed to be incompressible during impact (Rein, 1993; Yarin, 2006; Marengo *et al.*, 2011; Josserand and Thoroddsen, 2016).

The two-fluid Navier–Stokes equations

Both gas and liquid obey the incompressible Navier–Stokes equations (with respective densities and viscosities) with jump conditions at the interface. This complete dynamics can be described within the one-fluid formulation of the incompressible Navier–Stokes equation, which can be stated as follows:

$$\rho\left(\frac{\partial \mathbf{u}}{\partial t} + \mathbf{u}\nabla\mathbf{u}\right) = -\nabla p + \rho\mathbf{g} + \mu\triangle\mathbf{u} + \gamma\kappa\delta_s\mathbf{n} \qquad (1)$$

to which is added the equation of mass conservation, which for incompressible fluid yields

$$\nabla \cdot \mathbf{u} = 0 \qquad (2)$$

where $\mathbf{u}$ is the vector of fluid velocity, ∇ is the usual differential operator, p is the pressure field, with function of space $\mathbf{x}$ and time t, and $\triangle$ the Laplacian operator. In these equations, the density $\rho(\mathbf{x}, t)$ and viscosity $\mu(\mathbf{x}, t)$ are discontinuous fields of space and time. $\rho(\mathbf{x}, t)$ ($\mu(\mathbf{x}, t)$) is ρ_l or ρ_g (μ_l or μ_g) depending on whether we are in the liquid or gas phase. The term $\gamma\kappa\delta_s\mathbf{n}$ represents the surface tension force, proportional to the curvature κ and localized on the interface (the Dirac term δ_s) with normal is $\mathbf{n}$. The curvature is defined by the divergence of this vector:

$$\kappa = \nabla \cdot \mathbf{n}$$

An additional equation has to be considered for the motion of each phase (gas and liquid), leading eventually to the movement of the interface. Indeed, considering the characteristic function $\chi(\mathbf{x}, t)$, which is equal to one in the liquid phase and zero in the gas phase, the volume conservation of both phases implies that χ is the solution of the advection equation:

$$\frac{\partial \chi}{\partial t} + \mathbf{u} \cdot \nabla\chi = 0 \qquad (3)$$

Within this framework, both fluids satisfy the incompressible Navier–Stokes equation with the applicable density and viscosity.

From here on the soil surface is taken to be rigid. This simplification comes from the unavailability of a realistic deformation law for soils at the scale of a raindrop.

Numerical method and dimensionless version

The Navier–Stokes equations (1, 2, 3) are solved by the open source Gerris flow solver (version 2013/12/06) (Popinet, 2007). Gerris uses the Volume of Fluid method on an adaptive grid (Popinet, 2003, 2009). The rotational symmetry of the problem around the vertical axis is used to perform 2D numerical simulations using cylindrical coordinates (called 3D-axisymmetric coordinates).

The discretization of the equations is made on a quadtree structure for square cells. The quadtree structure allows for a dynamic mesh refinement: when needed, a 'parent' cell of the mesh is divided into four identical square 'children' cells (the length of which is half that of one of the parent cells), up to a maximum level n of refinement. Similarly, a cell merging is performed whenever the precision of the computation is below a user-defined threshold. The refinement/merging criterion is based on a mix of high values of the density and velocity gradients. Hence smaller cells are used at the gas/liquid interface and at locations showing large changes in velocity.

The interface between the gas and liquid phases is tracked using a color function C, which corresponds to the integral of the characteristic function in each grid cell. C is taken as the fraction of liquid phase inside the cell. This allows for the interface to be reconstructed using the piecewise linear interface calculation (Li, 1995), leading to a conservative advective scheme for the advection of the interface (Brackbill *et al.*, 1992; Lafaurie *et al.*, 1994). For each phase, the viscosities

(μ_g or μ_l) and the densities (ρ_g or ρ_l) are constant because the fluids are assumed incompressible. Hence each cell crossed by the interface has a viscosity μ and a density ρ determined by the relative volume fraction of each phase, as follows:

$$\rho = C\rho_l + (1-C)\rho_g; \quad \text{and} \quad \mu = C\mu_l + (1-C)\mu_g \tag{4}$$

Finally, the Navier–Stokes equations are solved in Gerris in a dimensionless form to lower numerical errors. The domain length has a size of one. The other lengths are rescaled by a factor λ using a numerical diameter of the raindrop $D' = 0.3$ in Gerris (so $\lambda = D/D'$), the velocities, densities, time and pressure by U_0, ρ_l, λ/U_0 and $\rho_l U_0^2$, respectively. Hence the effective Navier–Stokes equation to solve reads

$$\rho'\left(\frac{\partial \mathbf{u}'}{\partial t'} + \mathbf{u}'\nabla'\mathbf{u}'\right) = -\nabla' P' + \rho\mathbf{g}' + \mu'\triangle'\mathbf{u}' + \gamma'\kappa'\delta_s'\mathbf{n} \tag{5}$$

where the primes represent dimensionless variables.

Simulated cases and conditions

We performed numerical simulations for typical raindrop impacts falling on a water layer. All computations were done for spherical raindrops of diameter equal to $D = 2$mm. Considering the scaling factor $D' = 0.3$, this leads to a domain of 6.67 mm in both width and height. The raindrop velocity was set to its terminal velocity, U_0= 6.5 m s^1. The thickness of the water film h varied from $D/10$ (i.e. 0.2 mm) to $2D$ (i.e. 4 mm), with the intermediate cases $D/5$, $D/3$, $D/2$ and D.

Standard air and water properties were used: $\rho_l = 10^3$ kg m^{-3}, $\mu_l = 10^{-3}$ kg m^{-1} s^{-1}, $\rho_g = 1$kg m^{-3}, $\mu_g = 2 \times 10^{-5}$ kg m^{-1} s^{-1}, with a surface tension $\gamma = 0.02$ kg s^{-2}. In this configuration, the Reynolds number Re was 6500 and the Weber number We 2112.5. These large values indicate that inertia dominates a priori the other forces. Preliminary testing confirmed that the effect of gravity was negligible during a raindrop impact. Consequently, gravity was not included in the simulations.

At high velocities, drop impacts develop angular instabilities, leading to the well-known pictures of splashing popularized, for instance, in commercials. Splash is one of the key issues of drop impacts identified already by Worthington (1876) in the first studies on drop impacts, leading, for instance, to secondary droplet break-up (Rein, 1993). These splashing dynamics can be important in soil erosion because it can transport eroded material at large distances, as shown by Planchon and Mouche (2010). In the present case, the axisymmetric geometry can be used because (i) we are focusing on the erosion mechanism itself and not on the transport of particle, and (ii) such instabilities become relevant for timescales much larger than the typical timescale of the pressure and shear stress development at the soil surface. Consequently, an axial boundary condition was imposed on the symmetry axis ($r' = 0$). At the soil surface ($z' = 0$), a zero velocity boundary condition (also known as Dirichlet condition) was set. This ensured that both (i) no infiltration ($u_z' = 0$) and (ii) no slip ($u_r' = 0$) occurred. For the top ($z' = H'_{\max} = 1$) and radial ($r' = R'_{\max} = 1$) boundaries, either Neumann (no slip) or Dirichlet (zero velocity) boundary conditions could potentially be used. Preliminary testing showed that the type of boundary condition did not influence the results because the simulated domain was sufficiently large compared to the area of interest. For the simulations, a Dirichlet condition was used at $z' = H'_{\max}$ and $r' = R'_{\max}$.

During simulation of a raindrop impact, the water height h can become zero (especially for thin initial water depths). The occurrence of cells with $h = 0$ requires special attention, because it involves the motion of the contact line separating the water and the air along the soil surface (i.e. a triple-point occurs). In general, a specific boundary condition should be applied at the moving contact point to account for the high viscous stresses involved (Afkhami *et al.*, 2009). In our case, an alternative approach can be used by acknowledging that a real soil surface is not exactly smooth but involves some roughness, which can be crucial for the dynamics of the impact. This roughness can be taken into account by imposing a Navier slip boundary condition on the soil surface with a slip length of the order of the roughness (Barrat and Bocquet, 1999). Technically, since the usual no-slip boundary condition imposed by the numerical scheme corresponds to a Navier slip condition with a slip length of the order of the mesh size, one has simply to take the no-slip boundary condition here with a mesh size similar to the surface roughness. Therefore, the numerical no-slip boundary conditions imposed for a constant level of refinement can be interpreted as a natural model for the soil roughness. In that framework, throughout the simulations, we can consider that a surface roughness equal to 65 μm was used (level of refinement $n = 10$).

Results and Discussion

Overall dynamics

The phenomenology of a drop impact on a thin water layer is illustrated for the case $h = D/10$ in Figure 2, where the interface, the velocity and pressure fields are shown together for different times. In the following, the initial time $t' = 0$ is taken as the theoretical time of impact, defined by the falling velocity $U_0' = 1$ of a sphere onto the undeformed flat liquid layer.

At $t' = 10^{-3}$ (i.e. 1 μs after the impact initiation), the drop and the water layer are still separated by a narrow sheet of air (Figure 2a). Nevertheless, the pressure has started to increase in the water, mediated by the high lubrication pressure created in the cushioning air layer located between the drop and the liquid film. The maximum pressure ($P'_{\max} = 1.85$, i.e. $P_{\max} = 78.2$ kPa) is between the drop and the water layer.

At $t' = 10^{-2}$ (i.e. 10 μs after the impact initiation), the drop and the water layer have started to merge and some air is trapped inside the water (Figure 2b) due to the air cushioning (Thoroddsen *et al.*, 2003; Korobkin *et al.*, 2008). A high-pressure field is created, with a maximum pressure of $P'_{\max} = 2.68$ (i.e. $P_{\max} = 113.2$ kPa) now located close to the wedge formed by the intersection between the drop and the liquid layer. At $t' = 0.03$ (i.e. 31 μs after the impact initiation), most of the water that belonged to the raindrop still has its terminal velocity (Figure 2c). It is only in the impact region that the velocity vectors rotate from the vertical. In this same area, the velocities are smaller than the terminal velocity but in the small wedge region one can see the formation of a high-speed jet created by the high pressure peak. Indeed, the maximum pressure is still located near the wedge but has started to decrease ($P'_{\max} = 1.47$, i.e. $P_{\max} = 62.1$ kPa). A few droplets are emitted from the wedge.

At $t' = 0.08$ (i.e. at $t = 82\mu$s), a complex velocity field is formed (Figure 2d). Firstly, a jet has been emitted by the impact, leading to a splash of which the specific dynamics would be fully three dimensional and which is not at the heart of the present study. Secondly, close to the soil surface, the velocity field is expanding mostly radially due to the spreading of the raindrop into the water layer. Together with the

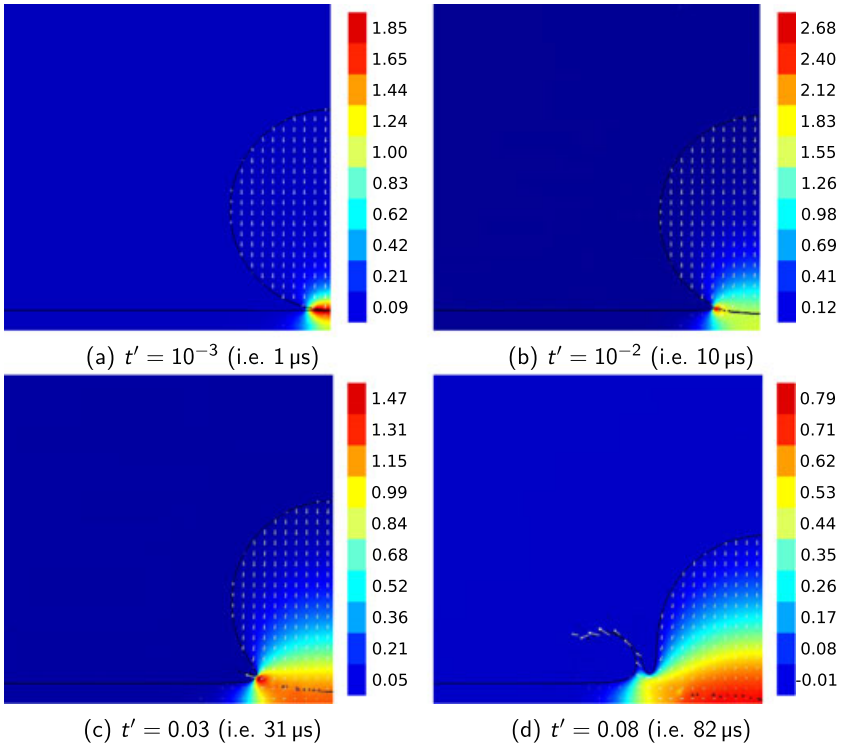

Figure 2. Pressure and velocity fields in the water (colors and arrows respectively) as a function of time for a film layer of $h = \frac{D}{10}$. The drop diameter is 2 mm with a terminal velocity of 6.5 m s^{-1}. $t' = 10^{-3}$ (i.e. 1 μs) $t' = 10^{-2}$ (i.e. 10 μs) $t' = 0.03$ (i.e. 31 μs) $t' = 0.08$ (i.e. 82 μs).

no-slip boundary condition on the soil surface, this leads to a radial velocity field depending both on the radius r' and the vertical coordinate z'. In fact, the no-slip boundary condition imposed at $z' = 0$ induces the formation of a viscous boundary layer between the substrate and the radial flow created by the impact (Roisman, 2009; Eggers *et al.*, 2010). Hence the soil is subjected to a significant shear stress, which is crucial for erosion processes. The pressure field is now maximal near the soil surface, directly under the impact region, but its maximum value has decreased to $P'_{\max} = 0.8$ (i.e. $P_{\max} = 33.8$ kPa).

This general description is in agreement with previous publications on raindrop impacts on a water layer (Wang and Wenzel, 1970; Ghadiri and Payne, 1977, 1980, 1986; Hartley and Alonso, 1991; Hartley and Julien, 1992; Marengo *et al.*, 2011).

Since the erosion rate depends mostly on the shear stress applied on the soil surface, a detailed analysis of the dynamical evolution of the stress tensor during the impact is needed. In particular, the Meyer-Peter and Müller equation is often used, relating the erosion rate q_s to the shear stress τ (Meyer-Peter and Müller, 1948; Houssais and Lajeunesse, 2012):

$$q'_s = c(\tau' - \tau'_c)^{3/2}$$

where the dimensionless erosion rate and shear stress are defined by

$$q'_s = \frac{q_s}{\sqrt{(\rho_s/\rho_l - 1)gd^3}} \quad \text{and} \quad \tau' = \frac{\tau}{(\rho_s - \rho_l)gd}$$

where d is the typical size of the grains composing the soil, ρ_s is its density and c is an empirical constant fitted through experimental data. In the following, we will use the numerical simulations done for raindrop conditions to deduce scaling laws for the shear stress induced by the impact that we will compare with simple formulas obtained using a self-similar model. Prior to the shear stress itself, we will investigate the pressure field created by the impact, where self-similar behavior has already been observed (Josserand and Zaleski, 2003). Here, self-similarity means that the pressure field depends only on a quantity that is time dependent. In particular, it means that the pressure field conserves the same shape with time, with only amplitude and size varying with time.

Pressure evolution inside the water and self-similar approach

In fluid mechanics, scaling laws have been deduced from numerical simulations of the pressure evolution inside the water during the impact of a droplet on a solid surface or in the limit of thin liquid films, using a self-similar approach (Josserand and Zaleski, 2003; Eggers *et al.*, 2010). However, their validity has not been studied in the context of raindrop impacts yet, in particular when the liquid film thickness varies. The self-similar approach is based on a theory first developed by Wagner (1932) using as the typical length scale involved in the impact the intersection between a falling spherical drop and the unperturbed liquid layer surface. In other words, the pertinent length scale of the impact $r_c(t)$ (or $r'_c(t')$ in dimensionless form) is as follows:

$$r_c \propto \sqrt{DU_0 t} \quad \text{or} \quad r'_c \propto \sqrt{t'} \tag{6}$$

where t (t') is the time after the contact of the falling drop on the surface. This formula corresponds to the intersection of the drop (taken as a circle of radius $D/2$) that is in contact with the water surface at time $t = 0$. The self-similar theory takes advantage of the observation on the numerical simulations that the perturbed region of the drop at a short time after impact is governed by r_c (Josserand and Zaleski, 2003). Such a self-similar approach is possible when no specific length scale is dominating the dynamics: this is precisely the situation at a

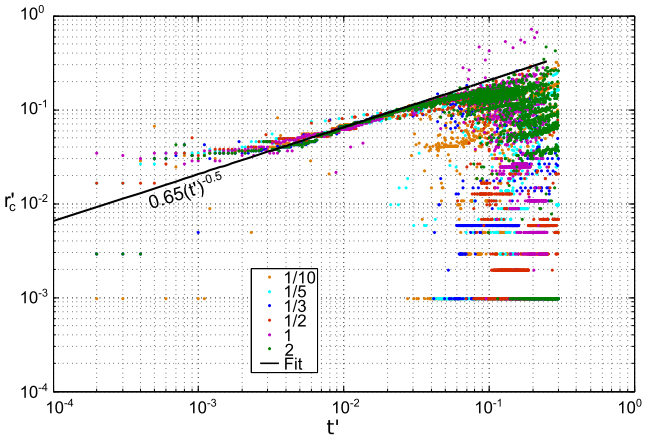

Figure 3. Position of the maximal dimensionless pressure as a function of time after impact for different water depth/drop diameter ratios. Note: the exponent was not fitted.

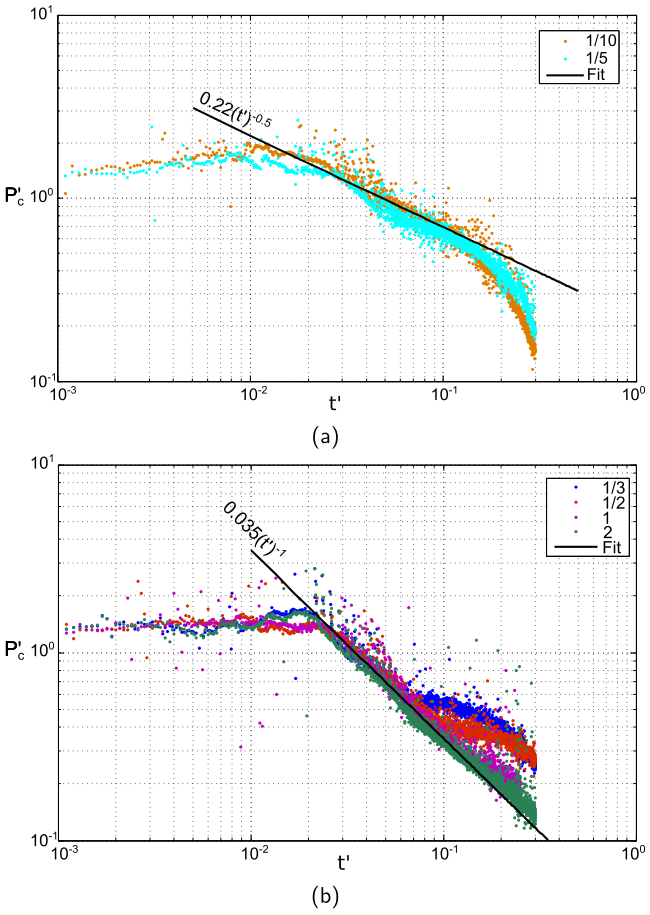

Figure 4. Maximum dimensionless pressure as a function of time for (a) small and (b) large water depth to drop diameter ratios. Note: the exponents were not fitted.

short time for high Reynolds and Weber numbers, where only the intersection between the falling drop and the impacting liquid layer is thus playing a role.

Indeed, Figure 3 shows the evolution with time of the radial position r'_c of the maximum pressure in the water for different liquid layer thicknesses. This evolution can be separated into three stages. For $t' < 2.10^{-3}$ (i.e. for durations smaller than 2.1 μs), the evolution of r'_c depends on the ratio h/D. This is also true for $t' > 2.10^{-2}$ (i.e. for durations larger than 20.5 μs), where it can also be noticed that, at the beginning of this period, r'_c is of the order of one raindrop radius (i.e. $r'_c = 0.15$ in Figure 3). In the intermediate stage, all the values of r'_c collapse onto a single straight line (in log-log scale), meaning that the relationship between the location of the maximum pressure and time is independent of the ratio h/D. Over this period, the position of the maximum pressure $r'_c(t')$ is in good agreement with the former square-root law (6), yielding quantitatively

$$r'_c = 0.65\sqrt{t'}$$

Remarkably, and as predicted by the theory, this law is independent of the layer thickness, in addition to being found independent of the Reynolds and Weber numbers in previous studies (as long as these numbers are high enough) (Thoroddsen, 2002; Josserand and Zaleski, 2003).

As geometrically deduced, this geometric law should not be valid for $r_c > D/2$. However, it is well known that the square-root law for r_c is in fact observed for much larger values and, in the figure, the law is typically valid up to $r_c \sim 2\ D$. Indeed, it has been argued that such a square-root law is also the cylindrical shock solution of the shallow-water equations as explained in Yarin and Weiss (1995), so that the geometric law matches this shock solution for longer times. The limitation of this regime at short and long times can be explained by two distinct arguments. At short timescales, the cushioning of the air layer delays the contact between the drop. At long timescales, numerical limitations can also be present: because the drop spreading has a large spatial extent, finite size effects coming from the size of the numerical box start to affect the dynamics.

Similar regimes are observed for the maximum pressure in the water P'_c, as shown on Figure 4. Firstly, the pressure is slightly varying at short timescales $t' < 2.10^{-2}$ (i.e. lower than 20.5 μs) and does not depend on the h/D ratio. At this stage the contact between the raindrop and the water layer is weak and we attribute this effect to the lubrication pressure created in the gas layer. At long timescales, typically corresponding to $r'_c > D/2$, the pressure rapidly drops to very small values. In between, corresponding roughly to $2.10^{-2} \leq t' \leq 10^{-1}$, the pressure decreases with time following power law behaviors. However, two distinct regimes are observed depending on the ratio h/D: for small aspect ratios (typically $h/D < 1/4$) the maximum pressure is found to decrease following the inverse of the square root of the time (Figure 4a), as usually observed for the impact on the thin liquid layer (Josserand and Zaleski, 2003). For thicker water layers (i.e. for $h/D \geqslant 1/4$), another regime is observed where the maximum pressure decreases first like the inverse of time (Figure 4b), while the inverse of the square root of the time seems to remain valid at longer times. The crossover between these two time dependences increases with the aspect ratio h/D.

As detailed in Josserand and Zaleski (2003), the thin water layer behavior can be understood using a simple momentum balance in the self-similar impact region. Indeed, it has been observed that in this regime the pressure field is perturbed in the impacted region only, defined by the characteristic length $r_c(t)$. Therefore, one can develop a self-similar approach using this length and perform the vertical momentum balance in the self-similar volume of radius $r_c(t)$ (the volume being that of a half-sphere of radius r_c, namely $2\pi r_c^3/3$), yielding

$$\frac{\mathrm{d}(2\rho_l \pi r_c(t)^3 U_0/3)}{\mathrm{d}t} \sim \pi r_c(t)^2 P_c(t)$$

where $P_c(t)$ is the typical amplitude of the pressure field created by the impact. This equation balances the variation of

vertical momentum in the self-similar half-sphere of radius $r_c(t)$ with the force of the pressure on the liquid layer, giving

$$P_c(t) \propto \rho_l U_0 \frac{\mathrm{d}r_c(t)}{\mathrm{d}t} \sim \rho_l U_0^2 \sqrt{\frac{D}{U_0 t}}$$

This regime is in good agreement with the observed maximum pressure evolution for thin liquid films (Figure 4a). Moreover, this regime starts to fail at a longer timescale (typically corresponding to $r_c(t) \sim D/2$) and the dynamics can then be described by the shallow-water equation (Yarin and Weiss, 1995; Lagubeau *et al.*, 2010).

For thick water layers, the former vertical momentum balance does not work since the liquid layer dynamics have to be taken into account. However, inspired by the former balance, one can deduce a simple model: considering that the radial characteristic length is still r_c but that the vertical one is now h, we obtain

$$\frac{\mathrm{d}(\rho_l \pi r_c(t)^2 h U_0)}{\mathrm{d}t} \sim \pi r_c(t)^2 P_c(t),$$

which gives the observed scaling for the pressure:

$$P_c(t) \sim \rho_l U_0 \frac{h}{r_c(t)} \frac{\mathrm{d}r_c(t)}{\mathrm{d}t} \sim \rho_l U_0^2 \frac{h}{U_0 t}$$

The former thin layer regime is retrieved at a longer timescale in this configuration and one can argue that this comes from the fact that the liquid contained in the layer has been pushed away by the impact so that only a thin residual liquid layer remains beneath the drop.

Therefore, we have shown that the pressure field due to the impact follows self-similar laws involving the spreading radius $r_c(t)$. However, as explained above, the crucial quantity for the erosion process is not the maximum pressure in the liquid but rather the shear stress at the soil surface. The self-similar approach can be used a priori to compute the soil surface quantities, but one has to notice that the soil surface does not coincide with the self-similar geometry (which involves the liquid layer interface rather than the solid surface). In conclusion, this leads to the difficult challenge of determining the shear stress at the intersection between the self-similar geometry and the soil surface. Moreover, the shear stress is also a consequence of the boundary layer created by the large-scale flow and the no-slip boundary condition imposed at the surface (Roisman, 2009; Eggers *et al.*, 2010; Lagubeau *et al.*, 2010), which makes its prediction even more difficult.

Scaling laws for stresses onto the soil surface

We therefore now investigate the pressure and shear stress fields onto the soil surface – quantities of interest for understanding and modeling erosion processes, keeping in mind the underlying self-similar structure of the impact.

Dependency of the maximum shear stress with water depth

First, let us mention that the dependence of the shear stress with the water depth has already been studied using numerical simulations by Hartley and Alonso (1991) and Hartley and Julien (1992), leading to an algebraic fitted relationship for the maximum (over time and space) shear stress at the soil surface, as a function of the Reynolds number and the water depth:

$$\tau_{\max} = 2.85 \rho_l U_0^2 \left(\frac{h}{D/2} + 1\right)^{-3.16} \mathrm{Re}^{-0.55} C_1 \qquad (7)$$

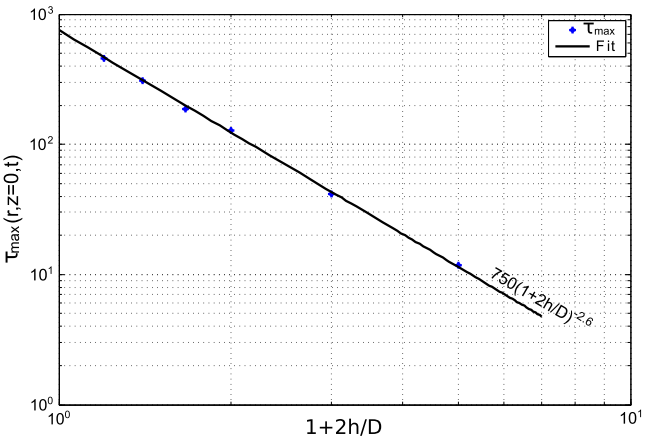

Figure 5. Maximum physical shear stress at the soil surface as a function of $(1 + 2h/D)$.

The prefactor C_1 is almost a constant number, varying only slightly with the impact parameters between 0.91 and 1 and deviating from one only for slow drops and thick water layers. However, this relationship was based on simulations that included only Reynolds numbers within the range 50–500 and Weber numbers in the range 18–1152 – values much lower than the range of natural raindrops ($6500 \leqslant \mathrm{Re} \leqslant 23000$, $50 \leqslant \mathrm{We} \leqslant 12150$). Hence their simulations underestimated the inertia forces compared to both viscous and capillary forces.

In the present study, we performed numerical simulations for realistic Re and We numbers for raindrops, varying only the water depth. Figure 5 shows the maximum shear stress $\tau_{\max}$ as a function of the liquid depth plus the drop radius normalized by the drop radius, which can be written as $1 + 2h/D$. It is well fitted by the following relationship:

$$\tau_{\max} \propto \left(\frac{h}{D/2} + 1\right)^{-2.6} \qquad (8)$$

The maximum shear stress is observed around the time $(D/2 + h)/U_0$, which would correspond to the penetration of half of the unperturbed drop over all the liquid layer. This relationship was fitted varying only the ratio h/D, so that the physical prefactor involves $\rho_l U_0^2$ multiplied by some function of the dimensionless numbers (in particular the Reynolds number). As far as the aspect ratio h/D is concerned, we observed that our fitted law is slightly different than the Hartley law (7), the exponent of the fraction being smaller. However, given the variation of $1 + 2h/D$ studied here, one should remark that the quantitative differences between our results and those of Hartley are not very large. In order to suggest an explanation for such dependence, a detailed study of the evolution of the stress tensor at the soil surface is first needed.

Self-similar evolution of the stress tensor on the soil surface

Pressure

The pressure field on the soil surface shows a bell-shaped curve with a maximum on the symmetry axis ($r = 0$) for all times, the amplitude of this curve decreasing with time, while its width increases. We thus define the characteristic length for the pressure field on the soil surface as the radius where the pressure is half the pressure on the axis $r'_{P_{1/2}}(t)$. The width

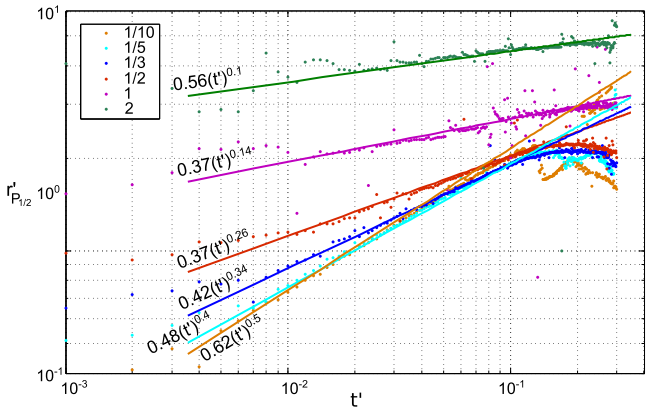

Figure 6. Dimensionless radial position $r'_{P_{1/2}}(t')$ of half the maximum dimensionless pressure (located at $r = 0$) at the soil surface for different ratios h/D shown in insert. The fitted power-law is traced on the figure for each value of h/D.

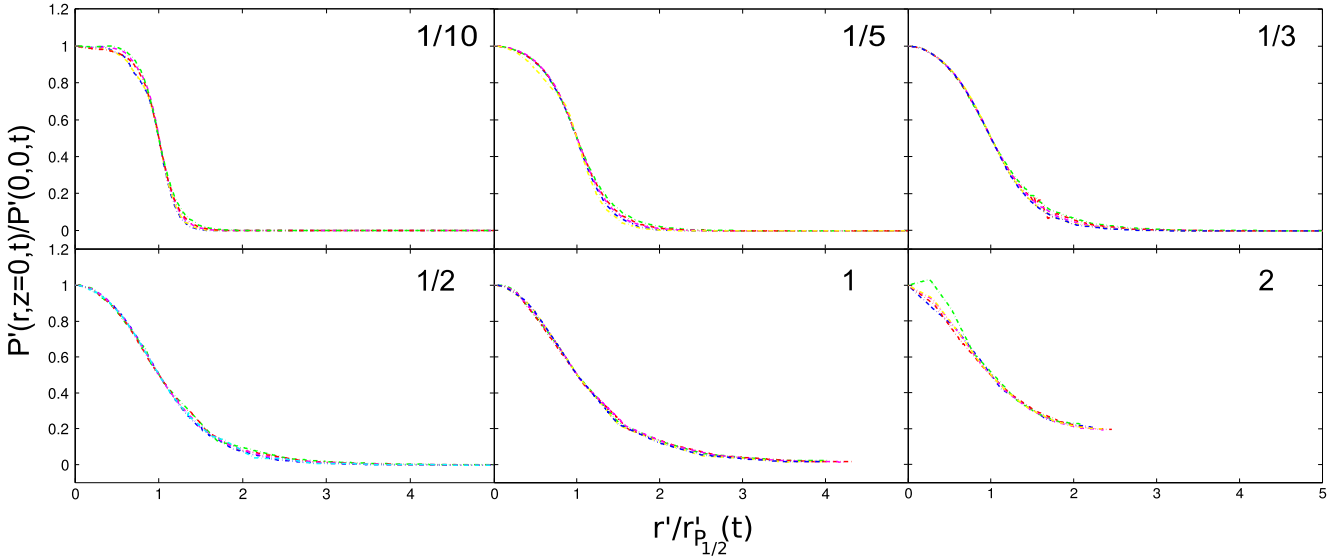

Figure 7. Rescaled pressure on the substrate for different aspect ratios h/D (indicated on each figure) for $t' < 10^{-1}$.

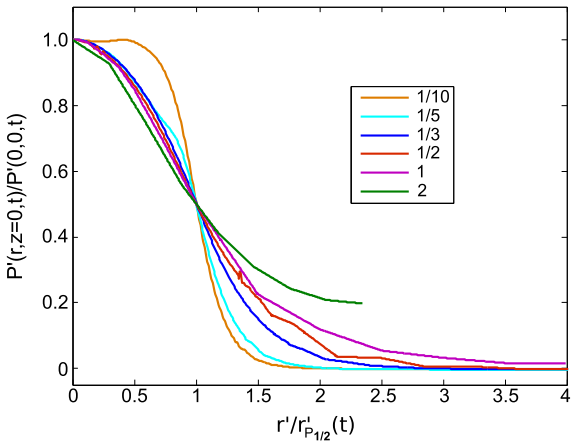

Figure 8. Comparison of the rescaled pressure for different aspect ratios h/D.

$r'_{P_{1/2}}(t')$ is shown in Figure 6 as a function of time for different aspect ratios h/D. For a short time after impact, the evolution of $r'_{P_{1/2}}(t)$ can be fitted by a power-law, the exponent m decreasing with the aspect ratio. For the thinnest simulated water layers, $r'_{P_{1/2}}(t)$ evolves as the square root of t' ($m \sim 0.5$), which is consistent with the law obtained for thin films. The exponent m of the power-law decreases when the water layer increases (see insert of Figure 6). Thus the water layer can be seen as a shield protecting the soil surface against the disturbance caused by raindrop impacts and it is only for the thinnest water layers, i.e. when the shielding is the lowest, that the disturbance (here the pressure) is similar inside the water layer and at the soil surface.

For deeper water layers, the shielding is more efficient, leading to a disconnection between the behavior of the pressure inside the liquid and at the soil surface. This disconnection becomes quite significant for a water layer equal to the drop radius.

However, a self-similar structure of the pressure field on the soil surface can also be exhibited for the different aspect ratios h/D. Indeed, rescaling the pressure on the soil surface $P'(r', z' = 0, t')$ at different times by the maximum value $P'(0, 0, t')$ and the coordinate r' by $r'_{P_{1/2}}(t)$, we observe a good collapse of the different pressure curves into a single one for $t' < 10^{-1}$ (i.e. smaller than 102.6 μs) (Figure 7). However, these self-similar curves vary with the aspect ratio h/D (Figure 8), the width e of the self-similar curve increasing with h/D.

Shear stress

The shear stress at the soil surface is computed numerically using the shear rate, yielding

$$\tau = \mu_l \frac{\mathrm{d}u_r(r, z = 0)}{\mathrm{d}z}$$

and it exhibits a ring shape of which the radius $r'_{\tau_{max}}(t')$, corresponding to the maximum shear stress location, increases with time. For thin liquid layers, $r'_{\tau_{max}}(t)$ evolves again approximately as the square root of t' (Figure 9a), while the situation is more complex for $h/D \geqslant 1$, where no tendency could be extrapolated (Figure 9b).

We rescaled again the dimensionless shear stress $\tau'(r, z = 0, t)$ by its maximum value (denoted by $\tau'_{max}(r, z = 0, t)$) and plotted it as a function of the rescaled radius $r'/r'_{\tau_{max}}(t)$ (where $r_{\tau'_{max}}(t)$ is the position of the maximum value of τ' at t) for short time $t' < 10^{-1}$ (i.e. smaller than 102.6 μs) (Figure 10).

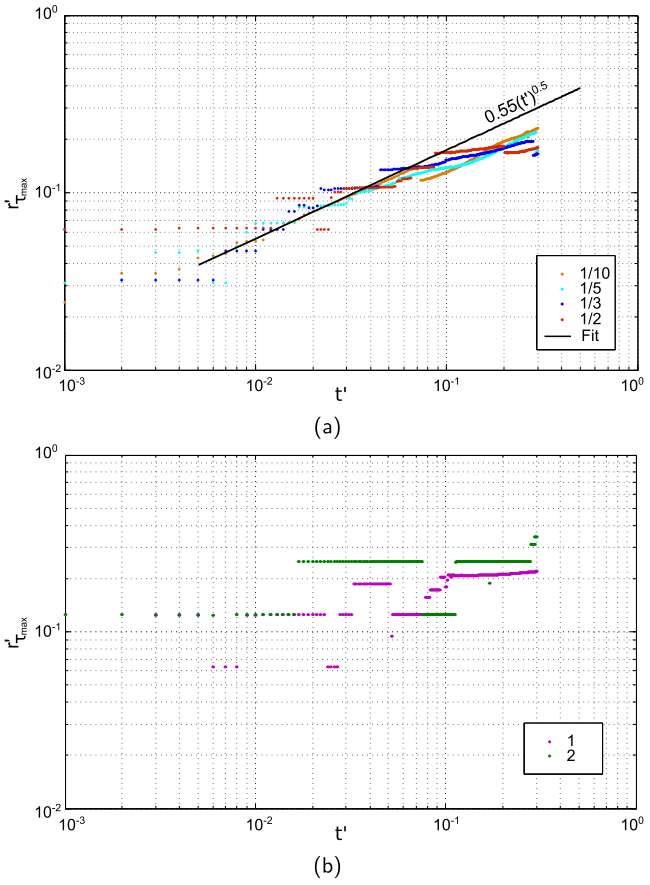

Figure 9. Time evolution of the dimensionless radial position $r'_{\tau_{max}(t)}$ of the maximum dimensionless shear stress at the soil surface for (a) small and (b) large h/D. Note: the exponent was not fitted.

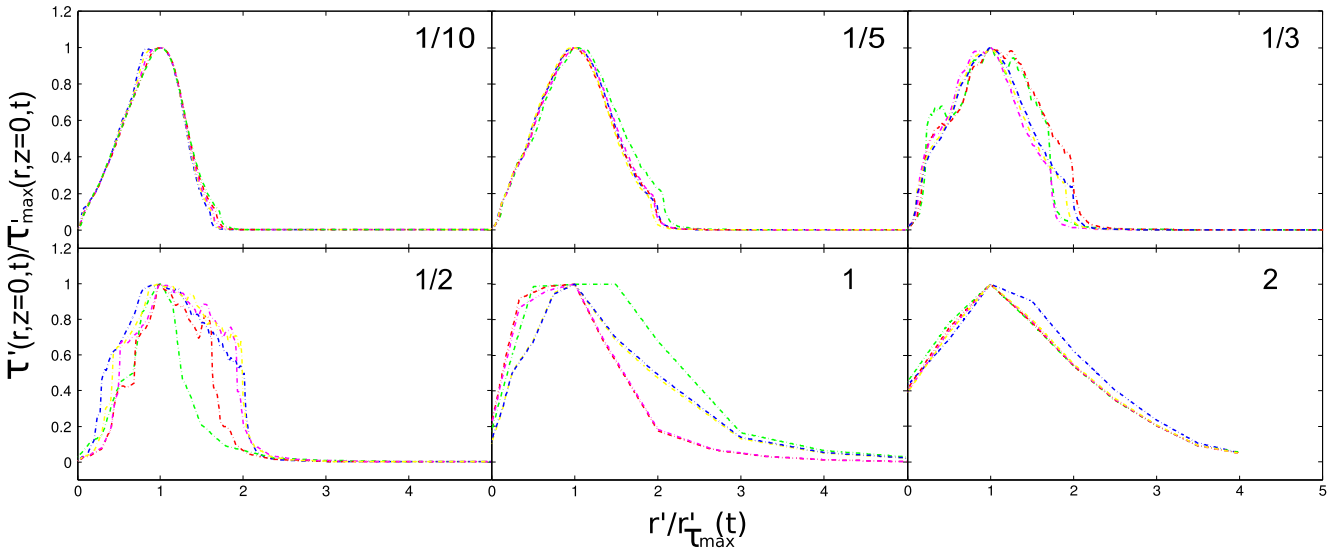

Figure 10. Rescaled dimensionless shear stress for different aspect ratios h/D for $t' < 10^{-1}$.

The collapse of the profiles is reasonable for small ($< 1/3$) and large (> 1) aspect ratios h/D but the situation is much more complex for intermediate cases, where only a partial collapse is found. The shear stress has a quasi-linear profile for small radius ($r' < r'_{\tau_{max}}(t)$) and then relaxes to zero for large r'. Such behavior for small radii can be understood within the dynamics of thin films (Yarin and Weiss, 1995; Lagubeau *et al.*, 2010). This regime is valid after the self-similar regime of the impact for which the pressure is high. Then, assuming a small gradient of the interface, the dynamics follow the so-called thin film equations, for which the radial velocity yields

$$u = \frac{r'}{t'}$$

for $r' < r'_{\tau_{\max}}(t)$. This radial velocity is not consistent with the no-slip boundary condition on the $z = 0$ solid boundary, so that a viscous boundary layer of thickness $l_v = \sqrt{\mu t/\rho}$ grows from the solid (Roisman, 2009; Eggers *et al.*, 2010). Therefore, one obtains for the shear stress on the solid (in dimensionless form)

$$\tau'(r, z = 0, t) \propto \frac{r'}{t'^{3/2}\mathrm{Re}^{1/2}}$$

which is consistent with the linear behavior for small r'. On the other hand, this regime can also explain the dependence of the maximum shear stress. Indeed, assuming that for the maximum shear stress obtained at time $t' = 1 + 2H/D$ the radial momentum of the thin film is equal to the vertical momentum of the impacting drop, one obtains approximately

$$D^3 U_0 \sim h_c D^2 U_0 \frac{(r'_{\tau_{\max}})^3}{t'_{\tau_{\max}}}$$

where h_c is the film height in the impacted zone, a priori different from the unperturbed film height h. Then, we obtain, taking the time of maximum shear stress at $t'_{\tau_{\max}} \propto 1 + 2h/D$

$$\frac{r'_{\tau_{\max}}}{1 + 2h/D} \sim \frac{1}{(r'_{\tau_{\max}})^2 h_c/D}$$

Then, using the observed relation $r'_{\tau_{max}} \propto \sqrt{t'_{\tau_{max}}}$, we have

$$\tau'_{\max} \propto \frac{1}{(1 + 2H/D)^{3/2} h_c/D}\mathrm{Re}^{-1/2}$$

Assuming the same scaling relation for the film height $h_c/D \propto 1 + 2h/D$ we obtain

$$\tau'_{\max} \propto \frac{1}{(1 + 2H/D)^{5/2}}\mathrm{Re}^{-1/2}$$

which is in good agreement with the numerical results. Note that the exponent $5/2$ is obtained from assumptions that are very speculative and which would need further studies to validate. However, it is very close to the 2.6 fitted exponent of relation (8), shedding light on the underlying mechanism for the film thickness that is at play in the shear stress formula. In particular, this exponent combines the contribution of the thin film velocity field with the viscous boundary layer. The $\mathrm{Re}^{-1/2}$ is a direct consequence of the boundary layer structure and thus has better scientific grounds although it has not been tested in our numerics. Note that it is in good agreement with the previous observed behavior (Hartley and Alonso, 1991; Hartley and Julien, 1992). We would like also to emphasize that such an analytical formula is very important since it could be implemented in macroscopic models coupling raindrops and erosion.

Conclusions

Using the present numerical methods to solve the Navier–Stokes equations for liquid–gas dynamics, we have studied raindrop impacts on water layers for realistic configurations. Quantities of interest for soil erosion, such as pressure and shear stress at the soil surface, have therefore been accurately computed, paving the way for quantitative understanding of soil erosion driven by rain.

The simulations confirm that the maximum shear stress at the soil surface depends in particular on the ratio between the water depth and the drop size. The variation of the pressure inside the water layer during the raindrop impact is well explained by a self-similar approach where the self-similar length is the spreading radius. The position of this radius corresponding to the maximum pressure moves as the square root of time after impact. Such a relationship comes from very general geometrical arguments and it was in fact previously observed numerically and experimentally for a wider range of drop impacts (especially with drop velocities different from the terminal velocity). Importantly, the present study shows that this relationship is independent of the ratio h/D.

At the soil surface, the maximum pressure is located at the center of the impact. Considering half of this pressure, it was found that it moves radially with the square root of the time after impact only for thin water layers $h/D < 1/5$. For low h/D ratios, the location of both the maximum pressure inside the water and the pressure at the soil surface follow the same law because the shielding caused by the water layer is minimal. The shielding becomes significant for larger h/D ratios, especially for $h/D \geqslant 1$, leading to a disconnection between pressure behaviors inside the water and at the soil surface. Nevertheless, for all h/D ratios, a self-similarity was found for the pressure rescaled by its central value $P(r, z = 0, t)$ as a function of the radius rescaled by the half-pressure radius. The existence of this self-similarity shows that the dynamics of the pressure at the soil surface are quite similar for different h/D ratios (even though the rescaling depends on h/D).

The shear stress at the soil surface was also rescaled, but the self-similarity was not as consistent as that for the pressure. This indicates that the dynamics of the shear stress is more complex, and that additional variables may have to be taken into account. In particular, one would need in a further study to elucidate the interplay between the growth of the viscous boundary layer and the spreading dynamics.

By clarifying the dynamics of the raindrop impact on a water layer, these results could foster experimental and numerical studies of soil erosion by raindrops. By identifying the variables of interest, it will simplify the design of these studies. More precisely, the equations for the maximum shear stress could be implemented in a macroscopic model of erosion to estimate the quantities of materials eroded. New insight could also come from theoretical developments carried out in fluid mechanics, such as the influence of air cushioning prior to the impact on the interface deformation (Xu *et al.*, 2005) or the changes in flow due to the granular structure of the soil.

Indeed, the biggest drawback of current numerical modeling is probably the hypothesis of a rigid soil surface, which comes from the unavailability of a suitable deformation law. To be realistic such a law should account for the aggregated status of soils. Finding such a law remains a challenge for soil physicists.

Acknowledgements— It is our pleasure to thank Leon Malan for his help. C.J. wishes to acknowledge the Agence Nationale de la Recherche through grant ANR 'TRAM' 13-BS09-0011-01.

References

Afkhami S, Zaleski S, Bussmann M. 2009. A mesh-dependent model for applying dynamic contact angles to vof simulations. *Journal of Computational Physics* **228**: 5370–5389.

Ahn S, Doerr SH, Douglas P, Bryant R, Hamlett CA, McHale G, Newton MI, Shirtcliffe NJ. 2013. Effects of hydrophobicity on splash erosion of model soil particles by a single water drop impact. *Earth Surface Processes and Landforms* **38**(11): 1225–1233.

Atlas D, Srivastava RC, Sekhon RS. 1973. Doppler radar characteristics of precipitation at vertical incidence. *Reviews of Geophysics and Space Physics* **11**(1): 1–35.

Barrat J-L, Bocquet L. 1999. Large slip effect at a nonwetting fluid–solid interface. *Physical Review Letters* **82**: 4671.

Brackbill J, Kothe DB, Zemach C. 1992. A continuum method for modeling surface tension. *Journal of Computational Physics* **100**: 335–354.

Bresson LM, Moran CJ. 2003. Role of compaction versus aggregate disruption on slumping and shrinking of repacked hardsetting seedbeds. *Soil Science* **168**(8): 585–594.

Charru F, Mouilleron H, Eiff O. 2004. Erosion and deposition of particles on a bed sheared by a viscous flow. *Journal of Fluid Mechanics* **519**: 55–80.

Dunne T, Malmon DV, Mudd SM. 2010. A rain splash transport equation assimilating field and laboratory measurements. *Journal of Geophysical Research – Earth Surface* **115**: 1–16.

Eggers J, Fontelos M, Josserand C, Zaleski S. 2010. Drop dynamics after impact on a solid wall: theory and simulations. *Physics of Fluids* **22**(062101): 1–13.

Erpul G, Gabriels D, Norton LD. 2004. Wind effects on sediment transport by raindrop-impacted shallow flow: a wind-tunnel study. *Earth Surface Processes and Landforms* **29**: 955–967.

Ferreira AG, Singer MJ. 1985. Energy-dissipation for water drop impact into shallow pools. *Soil Science Society of America Journal* **49**(6): 1537–1542.

Ferreira AG, Larock BE, Singer MJ. 1985. Computer-simulation of water drop impact in a 9.6-mm deep pool. *Soil Science Society of America Journal* **49**(6): 1502–1507.

Ghadiri H, Payne D. 1977. Raindrop impact stress and the breakdown of soil crumbs. *Journal of Soil Science* **28**: 247–258.

Ghadiri H, Payne D. 1980. *A study of soil splash using cine-photography*, De Boot M, Gabriels D (eds). Wiley: Chichester,185–192.

Ghadiri H, Payne D. 1986. The risk of leaving the soil surface unprotected against falling rain. *Soil and Tillage Research* **8**(1–4): 119–130.

Hartley DM, Alonso CV. 1991. Numerical study of the maximum boundary shear-stress induced by raindrop impact. *Water Resources Research* **27**(8): 1819–1826.

Hartley DM, Julien PY. 1992. Boundary shear-stress induced by raindrop impact. *Journal of Hydraulic Research* **30**(3): 341–359.

Houssais M, Lajeunesse E. 2012. Bedload transport of a bimodal sediment bed. *Journal of Geophysical Research* **117**: 1–13.

Huang C, Bradford JM, Cushman JH. 1982. A numerical study of raindrop impact phenomena: the elastic-deformation case. *Soil Science Society of America Journal* **47**(5): 855–861.

Josserand C, Thoroddsen S. 2016. Drop impact on a solid surface. *Annual Review of Fluid Mechanics* **48**: 365–391.

Josserand C, Zaleski S. 2003. Droplet splashing on a thin liquid film. *Physics of Fluids* **15**: 1650–1657.

Kinnell PIA. 1991. The effect of flow depth on sediment transport induced by raindrops impacting shallow flows. *Transactions of the ASAE* **34**(1): 161–168.

Korobkin AA, Ellis AS, Smith FT. 2008. Trapping of air in impact between a body and shallow water. *Journal of Fluid Mechanics* **611**: 365–394.

Lafaurie B, Nardone C, Scardovelli R, Zaleski S, Zanetti G. 1994. Modelling merging and fragmentation in multiphase flows with SURFER. *Journal of Computational Physics* **113**: 134–147.

Lagubeau G, Fontelos M, Josserand C, Maurel A, Pagneux V, Petitjeans P. 2010. Flower patterns in drop impact on thin liquid films. *Physical Review Letters* **105**(184503): 1–4.

Leguédois S, Planchon O, Legout C, Le Bissonnais Y. 2005. Splash projection distance for aggregated soils: theory and experiment. *Soil Science Society of America Journal* **69**(1): 30–37.

Lesser M, Field J. 1983. The impact of compressible liquids. *Annual Review of Fluid Mechanics* **15**: 97.

Li J. 1995. Calcul d'interface affine par morceaux [piecewise linear interface calculation]. *Comptes Rendus de l'Academie des Sciences,* Paris, série IIb **320**: 391–396.

Marengo M, Antonini C, Roisman IV, Tropea C. 2011. Drop collisions with simple and complex surfaces. *Current Opinion in Colloid and Interface Science* **16**(4): 292–302.

Meyer-Peter E, Müller R. 1948. Formulas for bed-load transport. In *Proceedings of the 2nd Meeting, International Association for Hydraulic Structures Research,* Stockholm,39–64.

Moss AJ, Green P. 1983. Movement of solids in air and water by raindrop impact: effects of drop-size and water-depth variations. *Australian Journal of Soil Research* **21**: 257–269.

Mouzai L, Bouhadef M. 2011. Shear strength of compacted soil: effects on splash erosion by single water drops. *Earth Surface Processes and Landforms* **36**(1): 87–96.

Mutchler CK, Young RA. 1975. Soil detachment by raindrops. In *Present Prospective Technology for Predicting Sediment Yields and Sources*, US Department of Agriculture: Washington, DC; 114–117.

Nearing MA, Bradford JM, Holtz RD. 1986. Measurement of force vs time relations for waterdrop impact. *Soil Science Society of America Journal* **50**(6): 1532–1536.

Nearing MA, Bradford JM, Holtz RD. 1987. Measurement of waterdrop impact pressure on soil surfaces. *Soil Science Society of America Journal* **51**: 1302–1306.

Palmer RS. 1963. The influence of a thin water layer on waterdrop impact forces. *International Association of Scientific Hydrology Publication* **65**: 141–148.

Palmer RS. 1965. Waterdrop impact forces. *Transactions of the ASAE* **8**: 69–70.

Parker G. 1990. Surface-based bedload transport relation for gravel rivers. *Journal of Hydraulic Research* **28**: 417–436.

Planchon O, Mouche E. 2010. A physical model for the action of raindrop erosion on soil microtopography. *Soil Science Society of America Journal* **74**: 1092–1103.

Popinet S. 2003. Gerris: a tree-based adaptive solver for the incompressible Euler equations in complex geometries. *Journal of Computational Physics* **190**(2): 572–600.

Popinet S. 2007. Gerris flow solver. http://gfs.sourceforge.net/.

Popinet S. 2009. An accurate adaptive solver for surface-tension-driven interfacial flows. *Journal of Computational Physics* **228**: 5838–5866.

Rein M. 1993. Phenomena of liquid drop impact on solid and liquid surfaces. *Fluid Dynamics Research* **12**: 61–93.

Roisman IV. 2009. Inertia dominated drop collisions. II. An analytical solution of the Navier–Stokes equations for a spreading viscous film. *Physics of Fluids* **21**(052104): 1–11.

Sharma PP, Gupta SC, Rawls WJ. 1991. Soil detachment by single raindrops of varying kinetic-energy. *Soil Science Society of America Journal* **55**(2): 301–307.

Singer MJ, Walker PH, Hutka J, Green P. 1981. Soil erosion under simulated rainfall and runoff at varying cover levels. *Technical report 55*, Division of Soils, Commonwealth Scientific and Industrial Research Organization Camberra, Australia.

Terry JP. 1998. A rainsplash component analysis to define mechanisms of soil detachment and transportation. *Australian Journal of Soil Research* **36**(3): 525–542.

Thoroddsen S. 2002. The ejecta sheet generated by the impact of a drop. *Journal of Fluid Mechanics* **45**(1): 373–381.

Thoroddsen ST, Etoh TG, Takehara K. 2003. Air entrapment under an impacting drop. *Journal of Fluid Mechanics* **478**: 125–134.

Thoroddsen ST, Eto TG, Takehara K, Ootsuka N, Hatsuki A. 2005. The air bubble entrapped under a drop impacting on a solid surface. *Journal of Fluid Mechanics* **545**: 203–212.

Torri D, Sfalanga M. 1986. Some aspects of soil erosion modeling. In *Agricultural Nonpoint Source Pollution: Model Selection and Application*, Giorgini A, Zingales F (eds), Elsevier: Amsterdam; 161–171.

Villermaux E, Bossa B. 2009. Single-drop fragmentation determines size distribution of raindrops. *Nature Physics* **5**: 697–702.

Wagner H. 1932. Über stoss und gleitvorgänge und der oberfläshe von flüssigkeiten. *Zeitschrift Angewandte Mathematik und Mechanik* **12**(4): 193–215.

Wang RC-T, Wenzel HG Jr. 1970. *The mechanics of a drop after striking a stagnant water layer. Technical report 30,* Water Resources Center, University of Illinois Urbana–Champaign, IL.

Worthington A. 1876. On the form assumed by drops of liquids falling vertically on a horizontal plate. *Proceedings of the Royal Society of London* **25**: 261–271.

Xu L, Zhang W, Nagel S. 2005. Drop splashing on a dry smooth surface. *Physical Review Letters* **94**(184505): 1–4.

Yarin AL. 2006. Drop impact dynamics: Splashing, spreading, receding, bouncing. *Annual Review of Fluid Mechanics* **38**: 159–192.

Yarin A, Weiss D. 1995. Impact of drops on solid surfaces: self-similar capillary waves, and splashing as a new type of kinematic discontinuity. *Journal of Fluid Mechanics* **283**: 141–173.